Electronic transport in magnetically ordered $Mn_5Si_3C_x$ films

B. Gopalakrishnan,[1,*] C. Sürgers,[1,2] R. Montbrun,[1] A. Singh,[1,†] M. Uhlarz,[1] and H. v. Löhneysen[1,2,3]
[1]*Physikalisches Institut, Universität Karlsruhe, D-76128 Karlsruhe, Germany*
[2]*DFG Center for Functional Nanostructures (CFN), Universität Karlsruhe, D-76128 Karlsruhe, Germany*
[3]*Forschungszentrum Karlsruhe, Institut für Festkörperphysik, D-76021 Karlsruhe, Germany*
(Received 8 November 2007; revised manuscript received 21 January 2008; published 11 March 2008)

$Mn_5Si_3C_x$ films exhibit antiferromagnetic or ferromagnetic behavior depending on the carbon doping level x. We report a detailed electronic-transport study of films prepared with different x. All films exhibit metallic behavior of the temperature-dependent resistivity $\rho(T)$ with a logarithmic increase towards low temperatures attributed to the structural disorder and the accompanied scattering of conduction electrons by two-level systems. Below 1 K, the Kondo-type behavior $\rho(T) \sim -\ln T$ shows a crossover to Fermi-liquid behavior $\rho \sim -T^2$ independent of the type of magnetic order. The magnetoelectronic properties such as Hall effect and magnetoresistance show clear differences characteristic for the different magnetically ordered phases, i.e., antiferromagnetic vs ferromagnetic.

DOI: 10.1103/PhysRevB.77.104414 PACS number(s): 68.55.−a, 72.15.Qm, 72.80.Ga, 73.50.−h

I. INTRODUCTION

The electronic properties of metal silicides are of continued interest due to their great potential in microelectronic applications. In particular, dilute magnetic semiconductors are proposed to hold great promise for semiconducting spintronic devices. Mn-doped semiconductors were predicted to show carrier-induced ferromagnetism reaching Curie temperatures above room temperature (RT) for GaN and ZnO hosts.[1] Apart from III-V and II-VI hosts, carrier-induced ferromagnetism was also reported for Mn_xSi_{1-x} (Ref. 2) and Mn_xGe_{1-x} films.[3] However, the preparation of such films is complicated due to the formation of thermodynamically favorable ferromagnetic Mn-Si clusters[4] or Mn_5Ge_3 precipitates[5] in the Si or Ge matrix, respectively. Mn_5Ge_3 films have been considered for spintronic applications due their metallic conductivity and easy implementation into the semiconductor-based device fabrication-technology.[6,7] Furthermore, the magneto-optical properties of $Mn_5(Ge_{1-x}M_x)_3$ (M=Sn,Pb) films were investigated in order to improve the low readout signals of Mn_5Ge_3.[8,9] Unfortunately, Mn_5Ge_3 has a low Curie temperature just barely above RT and the isostructural compound Mn_5Si_3 is an antiferromagnet. These are severe disadvantages when considering technological applications.

From a physics point of view, Mn-Si and Mn-Ge compounds are interesting due to the competing magnetic interactions leading to ferromagnetic, ferrimagnetic, or antiferromagnetic order. The magnetic structure of Mn_5Si_3 has been studied intensly for almost 40 years.[10–12] Mn_5Si_3 shows two different antiferromagnetic configurations with a low-temperature highly non-collinear phase.[12] In contrast, the moments of ferromagnetic Mn_5Ge_3 were reported to be aligned along the hexagonal c axis.[13] However, in Mn_5Ge_3, competing interactions can lead to different magnetic phases induced by pressure or structural distortions as inferred from a recent DFT calculation.[14] This demonstrates the delicate influence of the interatomic distances on the magnetic interactions in Mn-based compounds.

It was previously reported that antiferromagnetic Mn_5Si_3 can be driven into a ferromagnetic (or ferrimagnetic) state by insertion of carbon into the voids of Mn octahedra of the hexagonal structure.[15] Carbon-doped Mn-Si compounds are also formed during growth of Mn/C/Si triple layers,[16] C/Mn/C/Si multilayers,[17] and of Mn films on 4H-SiC (0001) substrates.[18] In particular, magnetron-sputtered $Mn_5Si_3C_x$ films with $x \approx 0.8$ have a Curie temperature $T_C = 350$ K (Ref. 19) well above room temperature and even higher than $T_C \approx 300$ K reported for Mn_5Ge_3. Likewise, T_C is enhanced in $Mn_5Ge_3C_x$ films with a maximum $T_C = 442$ K.[20] Hence, carbon doping of Mn_5Si_3 or Mn_5Ge_3 may provide a favorable way to fabricate magnetic films for semiconductor devices. In light of possible spintronic applications and fundamental understanding, it is therefore worthwhile to study the electronic transport properties of $Mn_5Si_3C_x$ films. A further aspect concerns the impact of structural disorder on the electronic transport in sputtered films.

This paper is organized as follows: After the experimental details reported in Sec. II, we briefly recapitulate the structural and magnetic properties of $Mn_5Si_3C_x$ films in Sec. III A. The temperature and thickness dependences of the electrical resistivity are presented and discussed in Sec. III B, followed by the disussion of the magnetoresistance (Sec. III C) and the Hall effect at 4.2 K (Sec. III D). The various results will be discussed along with the presentation of the experimental data, and will finally be summarized in Sec. IV.

II. EXPERIMENTAL DETAILS

Films were prepared by magnetron sputtering in 5×10^{-3} mbar Ar atmosphere (base pressure of 10^{-7} mbar) from elemental Mn, Si, and C targets as described earlier.[19] Single crystalline $(1\bar{1}02)$ oriented sapphire substrates were heated to a substrate temperature $T_S = 470\,^{\circ}$C. Sputtering rates were adjusted in order to obtain $Mn_5Si_3C_x$ films of hexagonal structure with a concentration range $x = 0-1.2$. Throughout this paper, films without carbon ($x=0$) will be entitled as Mn_5Si_3. In the present study, films of thickness $d = 30-100$ nm were prepared by sputtering through a mechanical mask defining a stripe of width $w = 1$ mm and length

$L=10$ mm connected to six planar contact areas of the same material for four-terminal resistance and Hall-effect measurements. After deposition the films were covered by 5–10 nm Si at RT to avoid rapid oxidation of the samples in ambient atmosphere.

The film structure was analyzed at RT in a standard powder diffractometer (Siemens D 500) with Cu K_α radiation ($\lambda=0.154$ nm) in θ-2θ Bragg-Brentano configuration.

The magnetic properties were determined by vibrating-sample magnetometry between 2.3 and 280 K and in a superconducting quantum interference device magnetometer operating up to temperatures of 400 K. For these measurements, films on 5×5 mm^2 substrates were prepared under identical conditions without using a mask. Magnetic hysteresis curves shown in this paper were obtained by subtracting the diamagnetic contribution $M=-\chi B$ of the 0.5 mm thick sapphire substrate from the raw $M(B)$ data, where χ was chosen in order to obtain a field independent magnetization at high fields. Therefore, it was not possible to resolve possible paramagnetic contributions arising from the $Mn_5Si_3C_x$ film.

The resistance was measured in a ^{4}He bath cryostat for temperatures $T=3-300$ K and in a ^{3}He/^{4}He dilution refrigerator between 30 mK and 3 K with applied magnetic fields up to 5 T.

III. RESULTS AND DISCUSSION

A. Structural and magnetic properties

In this section, we briefly summarize the structural and magnetic properties by presenting recently acquired data that were taken on planar $Mn_5Si_3C_x$ films that were prepared independently but under identical conditions as the samples on which the resistivity measurements were carried out. For further details, we refer to Ref. 19 and references therein.

At RT, the parent Mn_5Si_3 compound has a hexagonal $D8_8$ structure (space group $P6_3/mcm$) with 2 f.u./ unit cell.[12] Mn occupies two inequivalent crystallographic sites, Mn_I and Mn_{II}. Mn_5Si_3 has two antiferromagnetic (AF) phases, AF2 between the Néel temperature $T_{N2}=99$ K and $T_{N1}=66$ K and AF1 below T_{N1}.[11] The onset of long-range antiferromagnetic order at T_{N2} is accompanied by an orthorhombic distortion. The different sites give rise to different local magnetic moments for Mn_I and Mn_{II} and a complicated magnetic structure which is highly noncollinear below T_{N1}. However, in sputtered Mn_5Si_3 films, the orthorhombic distortion seems to be lacking as inferred from the extended x-ray absorption fine structure (EXAFS).[19]

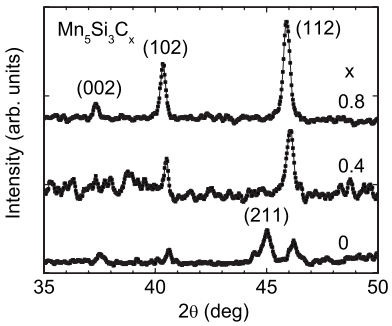

FIG. 1. θ-2θ x-ray scans (Cu K_α radiation) of 100 nm thick $Mn_5Si_3C_x$ films.

In $Mn_5Si_3C_x$, carbon is incorporated into the voids of the Mn_{II} octahedra (so-called "Nowotny phase").[15] Figure 1 shows the x-ray diffractograms of three $Mn_5Si_3C_x$ films with different carbon concentrations x. The prominent peaks are attributed to the (002), (102), (211), and (112) Bragg reflections of the Mn_5Si_3 phase. The small number of measured reflections is due to the texture of the films along the surface normal. Indeed, the complete diffraction pattern of the Mn_5Si_3 phase was obtained for powdered films dissolved from a NaCl substrate.[21] The shift of reflections to lower diffraction angles directly shows that the hexagonal lattice expands with increasing x corresponding to an (anisotropic) expansion — as inferred from EXAFS (Ref. 19) — of the unit cell by $\approx0.5\%-1\%$ of $Mn_5Si_3C_{0.8}$ compared to Mn_5Si_3.

The surface of the films exhibits a coarsely grained morphology as seen in scanning electron micrographs (Fig. 2) with a larger grain size for the thicker than for the thinner film. This suggests that the average grain size increases with film thickness d which is typical of evaporated thin films but is always much smaller than the film thickness.

The incorporation of carbon into the antiferromagnetic Mn_5Si_3 compound gives rise to a ferromagnetic magnetization curve with a maximum (average) Mn moment of $\approx1\mu_B$ and a Curie temperature $T_C=352$ K for $Mn_5Si_3C_x$ with $x=0.8-1$. As an example, Fig. 3(a) shows the magnetization M of ferromagnetic films with $x=0.4$ and 0.8 vs temperature T recorded in a weak magnetic field of $B=10$ mT. For $x=0.8$, the range $T\approx0-120$ K can be successfully described

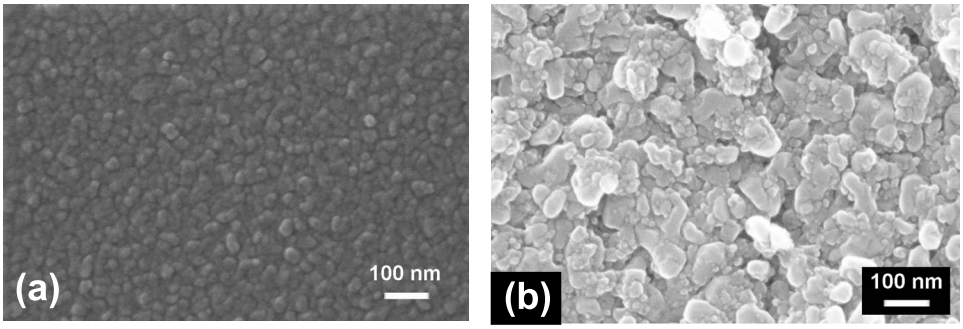

FIG. 2. Scanning electron micrographs of two $Mn_5Si_3C_{0.8}$ fims of (a) 30 nm and (b) 400 nm thickness.

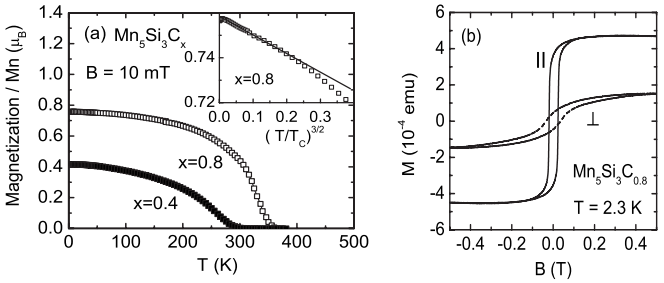

FIG. 3. (a) Magnetization $M(T)$ of two 100 nm $Mn_5Si_3C_x$ films in an applied field of 10 mT. Inset shows a plot M vs $(T/T_C)^{3/2}$ (T_C=350 K) for x=0.8 with the solid line indicating a linear behavior due to ferromagnetic spin waves. (b) Magnetic hysteresis loops of $Mn_5Si_3C_{0.8}$ with the magnetic field B applied parallel (solid line) and perpendicularly (dashed line) to the film plane.

by Bloch's law for the spontaneous magnetization $M(T)/M(0) \sim 1 - aT^{3/2}$ arising from ferromagnetic spin waves [see inset of Fig. 3(a)]. It is presently not clear whether the low average Mn moment is intrinsic, i.e., identical on the two Mn sites, or more likely due to a ferrimagnetic alignment of different Mn moments. In addition, a noncollinear alignment as reported for the AF1 phase of Mn_5Si_3 (Ref. 12) and calculated for Mn_5Ge_3 (Ref. 14) is also possible. We mention that the average magnetization of the films decreases with prolonged time after deposition, possibly due to an increasing oxidation from the outer surface toward the substrate during sample handling between the different measurements in ambient atmosphere. The largest average Mn moments were always obtained for $Mn_5Si_3C_x$ films with x =0.8 directly measured after deposition without delay.

Typical coercive fields derived from low temperature $M(B)$ loops are of the order of 50 mT for the optimum concentration x=0.8 [see Fig. 3(b)]. For this particular sample, a weak out-of-plane magnetization $M_\perp(B)$ was recorded with the field applied perpendicularly to the film. However, the absolute value of $M_\perp$ depends on the degree of texture and varies from sample to sample and quite often a hard axis loop is recorded for $M(B_\perp)$ as well (see also the discussion in Sec. III D).

B. Temperature dependence of resistivity

1. High temperatures $T > 30$ K

Figure 4 gives an overview of the resistivity ρ vs temperature T for 100 nm thick $Mn_5Si_3C_x$ films of different x. All films exhibit an increase of $\rho(T)$ with increasing temperature, i.e., a metallic behavior, with fairly high resistivities. $\rho(T)$ can be conveniently separated into

$$\rho(T) = \rho_{\min} + \tilde{\rho}(T), \tag{1}$$

where $\rho_{\min} = \rho(T_{\min})$ is the minimum resistivity measured at $T_{\min}$=10–20 K [see Fig. 7(b)] due to scattering by nonmagnetic impurities and structural imperfections and $\tilde{\rho}(T)$ represents the T-dependent part of $\rho(T)$. Here, we neglect the small upturn $\Delta\rho$ of the resistivity towards low T, observed below 30 K in several samples, which will be discussed in

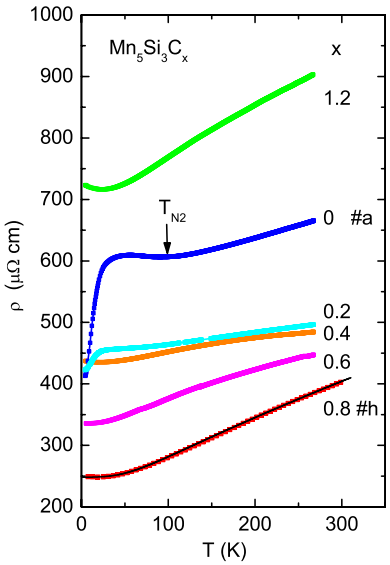

FIG. 4. (Color online) Resistivity ρ vs temperature T for 100 nm thick $Mn_5Si_3C_x$ films with different carbon concentrations x. Solid line for x=0.8 shows a calculation of $\rho(T)$ according to Eq. (2).

Sec. III B 2. Figure 4 immediately shows that $\rho_{\min}$ and the slope of the nearly linear T dependence do not exhibit a monotonic behavior as a function of the C concentration x (see Table I for details). The dependences of $\rho_{\min}$ and the resistance ratio (RRR) on the concentration x, together with the low-T logarithmic derivative of $\Delta\rho/\rho_{\min}$, are plotted in Fig. 5.

For x=0, i.e., the antiferromagnetic Mn_5Si_3, the temperature dependence is remarkably different from that of $Mn_5Si_3C_x$ films with $x \geqslant 0.4$. Below ≈100 K, $\rho(T)$ of Mn_5Si_3 deviates from a nearly linear dependence and shows an increase with decreasing T down to ≈50 K. This is apparently due to the onset of antiferromagnetic order at the Néel temperature T_{N2}=99 K (see arrow in Fig. 4) and indicates a spin-density-wave-like ordering with a gap opening on parts of the Fermi surface.[22] The qualitative behavior of $\rho(T)$ is similar to that of bulk Mn_5Si_3 polycrystals[23] with $\rho_{\min}$ =156 $\mu\Omega$ cm and to single crystals[24] with $\rho_{\min}(a,b$ axis) =150 $\mu\Omega$ cm and $\rho_{\min}(c$ axis)=50 $\mu\Omega$ cm. The high values of $\rho_{\min}$ therefore appear to be characteristic for Mn_5Si_3. In the present case of sputtered Mn_5Si_3 films, the enhanced $\rho_{\min}$=400 $\mu\Omega$ cm compared to bulk samples is likely to be due to a strong contribution of grain-boundary scattering.

For x=0.2, the linear $\rho(T)$ behavior prevails down to T ≈70 K (Fig. 4) with a remaining shoulder at ≈30 K. This shoulder disappears for higher concentrations $x \geqslant 0.4$. Note that films with x=0.2 already exhibit a ferromagnetism with a Curie temperature of $T_C \approx 200$ K (Ref. 21) and an average moment of $0.5\mu_B$/Mn. Yet, no indication of a kink in $\rho(T)$ (or $d\rho/dT$) for $T < T_C$ is found that would be reminiscent of a phase transition.[25] Therefore, it cannot be excluded that this shoulder in $\rho(T)$ remains from a minor AF phase for x=0.2 instead of being characteristic for the ferromagnetic phase.

While the x=0.2 data still bear some resemblance to those for x=0, the shoulder in $\rho(T)$ disappears for samples with x=0.4–1.2 which have a T_C higher than 270 K. Hence, in

TABLE I. Electronic-transport parameters of $Mn_5Si_3C_x$ films. x, carbon concentration; d, film thickness; ρ_{min}, minimum resistivity; RRR$=\rho(270\ \mathrm{K})/\rho_{min}$, resistance ratio; $\alpha=\frac{d(\Delta\rho/\rho)}{d\ln(T/T_{min})}$; $\gamma=\frac{d\Delta\sigma_s}{d\ln(T/T_{min})}$; and n.d.=not determined.

Sample	x	d (nm)	ρ_{min} ($\mu\Omega$ cm)	RRR	α (10^{-3})	γ ($10^{-5}\ \Omega^{-1}$)
a	0	100	413.1	1.611	n.d.	n.d.
b	0	100	424.5	1.136	−1.13	2.66
c	0.2	100	422.5	1.175	n.d.	n.d.
d	0.4	100	435.3	1.113	−3.47	7.80
e	0.6	100	335.8	1.332	−0.14	0.40
f	0.8	30	1640	1.293	−4.58	0.84
g	0.8	100	244.4	1.524	−1.78	7.26
h	0.8	100	248.6	1.557	−2.01	8.09
i	0.8	165	191.0	n.d.	−1.41	12.2
k	1.2	100	716.4	1.260	−6.37	8.90

$Mn_5Si_3C_x$ films, the change of the magnetic order from antiferromagnetic ($x=0$) to ferromagnetic ($x\geqslant 0.4$) is accompanied by a distinct change of the $\rho(T)$ behavior. Apart from the low-temperature behavior to be discussed below, samples with $x\geqslant 0.4$ exhibit a convex (negative) curvature with a maximum deviation from a strictly linear T dependence around 150 K. A similar behavior of $\rho(T)$ has been also reported for isostructural ferromagnetic Mn_5Ge_3 films.[6,26] A deviation from linearity is known for nonmagnetic transition metals as well and can have different reasons. First, according to Mott,[27] in transition metals, the electron s, p, and d states are strongly hybridized at low temperatures. The Fermi surface is considered to include an s-like part, which carries most of the current and a more localized d-like part, which determines the scattering. The relaxation time is mainly determined by the scattering into the d band where the electronic density of states (DOS) is high. Indeed, a self-consistent calculation for bulk Mn_5Si_3 shows that the Si p states and Mn d states are strongly hybridized and the total DOS near E_F is dominated by $N_d(E)$, with Mn_{II} d states being more localized than itinerant Mn_I states.[24] This is supported by photoemission data.[28] The strong variation of the d-band DOS $N_d(E)$ near the Fermi level gives rise to a behavior $\rho\sim T(1-AT^2)$, where A depends on $[dN_d(E)/dE]_{E_F}/N_d$. Consequently, a convex curvature is observed in Pd due to its high electronic DOS $N_d(E)$.

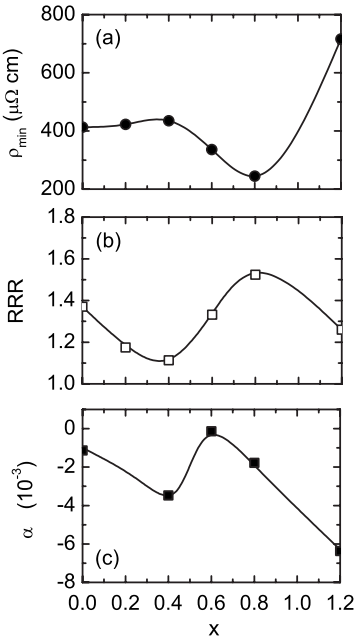

FIG. 5. Concentration dependence of (a) minimum resistivity ρ_{min}, (b) resistance ratio RRR$=\rho$ (270 K)$/\rho_{min}$, and (c) slope α of the logarithmic behavior $\Delta\rho/\rho_{min}=\alpha\ln(T/T_{min})$ at low T for 100 nm thick films. RRR data point for $x=0$ in (b) represents the average over two samples. Solid lines serve as guides to the eye.

In order to look for the existence of a contribution $\sim -T^3$ arising from s-d scattering, the resistivity of sample h ($x=0.8$) was calculated by application of a generalized Bloch-Grüneisen-Mott expression[29] with power $n=3$,

$$\rho(T)=\rho_{min}^{fit}+C\left(\frac{T}{\theta_D}\right)^n\int_0^{\theta_D/T}\frac{x^n}{(e^x-1)(1-e^{-x})}dx-BT^3, \tag{2}$$

where the second term arises from electron-phonon scattering yielding a behavior $\rho\sim T$ at high T, θ_D is the Debye temperature, and B represents a correction due to s-d transitions. The data of sample h are very well described by Eq. (2) with $\rho_{min}^{fit}=248\ \mu\Omega\ \mathrm{cm}\approx\rho_{min}$ (Table I), $\theta_D=390$ K close to the value of 377 K of bulk Mn_5Si_3,[30] $C=492.3\ \mu\Omega$ cm, and $B=1.5\times 10^{-7}\ \mu\Omega\ \mathrm{cm/K^3}$ [see the lowest curve ($x=0$) in Fig. 4].

A second reason for the negative curvature of the resistivity can be an incipient saturation of the resistivity at high T, which is typically found for systems where s-d interband transitions are important.[31] Clearly, the Boltzmann equation which, by the way, only considers intraband transitions, cannot be used to describe the resistivity saturation close to the Joffe-Regel limit where the electron mean free path (MFP) l approaches interatomic distances. However, early theoretical

work on resistivity saturation did not reach a consensus about the dominant mechanism. More recently, a theory has been developed by using the f-sum rule which is able to explain most of the effects concerning resistivity saturation in transition-metal compounds.[31] For the present case of $Mn_5Si_3C_{0.8}$ films, a maximum metallic resistivity of 750 $\mu\Omega$ cm is estimated according to the Joffe-Regel criterion[31] $k_F l \gg 1$ with $l \approx a$ the interatomic distance by assuming a three-dimensional spherical Fermi surface, a carrier (hole) density of $n=2.5\times10^{22}$ cm^{-3} (Sec. III D), and $a \approx 0.2$ nm. In fact, apart from the highly overdoped film with $x=1.2$ which is likely to be an inhomogeneous two-component mixture, all films satisfy the Joffe-Regel criterion. In this case, a model of weakly correlated electrons in a broad band of width $W \gg k_B T$ yields a resistivity saturation at high T (Ref. 31) and qualitatively explains the deviation from linearity.

We note that an estimate of the MFP for bulk Mn_5Si_3 from literature values of the total DOS $N(E_F)=7.26$ eV^{-1} at^{-1},[30] a Fermi velocity $v_F=2\times10^8$ cm/s derived from $E_F=11.6$ eV,[24] and $\rho_0=156$ $\mu\Omega$ cm (Ref. 23) via the free-electron expression,

$$l = \frac{3}{e^2 v_F N(E_F) \rho_{\min}} \tag{3}$$

(e the electron charge), leads to an unphysically small value of $l=0.01$ nm. On the other hand, these bulk materials[23,24] are still in the metallic region as judged from the fact that $d\rho/dT>0$ and, furthermore, have *lower* values of $\rho_{\min}$ than ≈ 250 $\mu\Omega$ cm ($x=0.8$) and 400 $\mu\Omega$ cm ($x=0$) of the $Mn_5Si_3C_x$ films (see Table I). This discrepancy illustrates that caution is necessary when treating complex transition-metal alloys within the free-electron model.

Of course, the models discussed so far do not consider the additional scattering of electrons by spin waves in the magnetically ordered material which are important at low temperatures as will be discussed in the following section.

2. Low temperatures $T<30$ K

Besides the temperature-dependent electron-phonon scattering discussed in the previous section, the contribution of electron–spin-wave scattering to the total resistivity can be strong in magnetically ordered materials[32] depending on the type of magnetic order and magnetic anisotropy (exchange or single-ion anisotropy), the latter giving rise to an energy gap ΔE_m in the excitation spectrum.

Figure 6(a) shows the low-temperature behavior of an antiferromagnetic Mn_5Si_3 film which can be described by

$$\rho(T) = \rho(0) + AT^2, \tag{4}$$

yielding $\rho(0)=399.4$ $\mu\Omega$ cm and $A=0.666$ $\mu\Omega$ cm/K^2, while for bulk Mn_5Si_3 polycrystals a behavior $\rho(T)=\rho(0)+A'T^{1.42}$ was reported.[23] In an *antiferromagnet*, the dispersion of spin-wave excitations is given by $\omega(k) \sim \sqrt{\Delta E_m^2 + Dk^2}$, where D is the spin-wave stiffness.[33] In isotropic, i.e., gapless case with $\Delta E_m \ll \sqrt{D}k$, the temperature dependence of ρ obeys a behavior $\rho \sim T^2$ as in the isotropic ferromagnetic case.[34,35] We tried to model the low-temperature behavior of $\rho(T)$ for the antiferromagnetic Mn_5Si_3 film [Fig. 6(a)]. Apart from the T^2 behavior of an isotropic antiferromagnet, no reasonable result could be obtained by fitting the case of an anisotropic antiferromagnet to the data.[33] The reason for the weak (or even zero) anisotropy could be the disorder of the coarsely grained films.

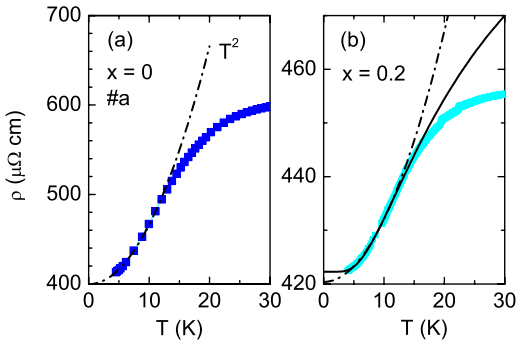

FIG. 6. (Color online) Low-temperature behavior of $\rho(T)$ for $Mn_5Si_3C_x$ films with (a) $x=0$ and (b) $x=0.2$. Dashed-dotted lines indicate a behavior $\rho \sim T^2$ [Eq. (4)] and solid line indicates a behavior described by Eq. (5).

For an isotropic metallic *ferromagnet*, a behavior $\rho \sim T^2$ is expected due to scattering of electrons by spin waves with dispersion $\omega(k) \sim k^2$ according to Kasuya[36] and Mannari.[37] This behavior is exemplified in MnSi single crystals with a high RRR ≈ 243 (Ref. 38). For an anisotropic ferromagnet, spin waves are only excited for energies larger than the energy gap $\Delta E_m'$ and therefore[39]

$$\rho(T) \sim T^2 \exp(-\Delta E_m'/k_B T). \tag{5}$$

For the ferromagnetic $Mn_5Si_3C_{0.2}$ film [Fig. 6(b)], the data can be described by the case of an isotropic ferromagnetic [Eq. (4)] with a coefficient $A=0.117$ $\mu\Omega$ cm/K^2 or by the case of an anisotropic ferromagnet with a small energy gap $\Delta E_m'/k_B=24$ K [Eq. (5)]. Apparently, the anisotropic case gives a better agreement to the data in a larger T range than the simple T^2 law for an isotropic ferromagnet [see Fig. 6(b)]. However, the occurrence of a shoulder of $\rho(T)$ (Fig. 4) characteristic of the antiferromagnetic material renders a clear conclusion impossible.

The single-band approximation by Kasuya[36] and Mannari[37] which describes the scattering of conduction electrons by ferromagnetic spin waves neglects interband scattering between the s conduction-electron band and the d band with different Fermi momenta k_{F1} and k_{F2}.[40] Such transitions require spin waves with wave vectors $k > k_{F1} - k_{F2}$. These are not populated at low temperatures and therefore the single-band approximation with $\rho \sim T^2$ provides an adequate description at low temperatures. The contribution from s-d transitions can be significant at higher temperatures. This is the reason why in a number of ferromagnetic materials and in the present case (Sec. III B 1) the low-temperature T^2 behavior of ρ crosses over to a nearly linear dependence at higher temperatures (but still well below the critical region).[32]

So far, we have neglected a weak logarithmic increase of $\rho(T)$ with decreasing T below ≈ 20 K. Figure 7(a) shows the

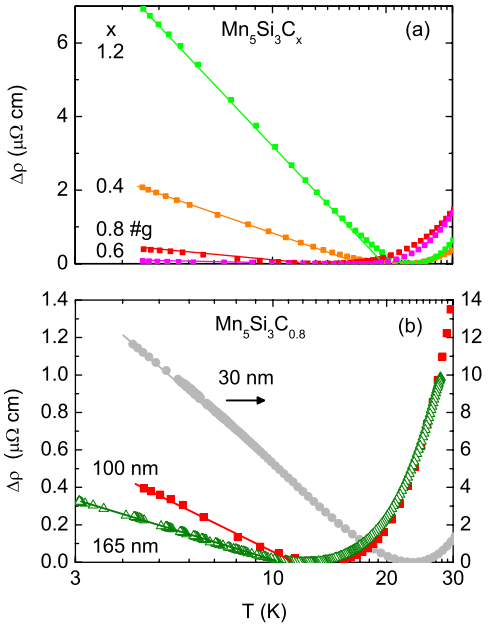

FIG. 7. (Color online) (a) Semilogarithmic plot of the excess resistivity $\Delta\rho=\rho(T)-\rho_{\min}$ for $Mn_5Si_3C_x$ films with $x\geqslant 0.4$. (b) Semilogarithmic plot of the excess resistivity $\Delta\rho$ for $Mn_5Si_3C_{0.8}$ films of different film thickness d. Solid lines show a behavior $\Delta\rho\sim-\ln T$.

low-temperature excess resistivity $\Delta\rho=\rho(T)-\rho_{\min}$ in a semilogarithmic plot. The slope α of the logarithmic behavior $\Delta\rho/\rho_{\min}=\alpha\ln(T/T_{\min})$, where $T_{\min}$ is defined by $\Delta\rho(T_{\min})=0$, depends on the concentration x and is smallest for $x=0.6$, i.e., near the optimum doping level (see Fig. 5).

Figure 7(b) shows $\Delta\rho$ for $Mn_5Si_3C_{0.8}$ films of different thicknesses d. Clearly, the logarithmic slope of $\Delta\rho$ increases with decreasing film thickness d. This suggests that the structural disorder, which is larger in thinner films containing smaller grains and a larger number of grain boundaries (see Fig. 2), is responsible for the logarithmic behavior. This interpretation is supported by the strongly increased $\rho_{\min}$ in the 30 nm film (c.f., Table I). Note that the data do not follow the Fuchs-Sondheimer theory[41] which predicts $\rho_{\min}\sim 1/d$.

$\rho(T)$ for a 165 nm thick $Mn_5Si_3C_{0.8}$ film is shown in Fig. 8 for various magnetic fields B applied perpendicularly to the film plane. Remarkably, the logarithmic slope does not depend on the magnetic field, apart from a vertical shift of the $\rho(T)$ curve toward lower resistivity. This negative magnetoresistance will be disccussed in Sec. III C.

Currently, four different phenomena are known that would give rise to an increase of the resistivity of a metallic film toward lower temperatures: (i) weak localization, (ii) enhanced electron-electron interaction, (iii) magnetic Kondo effect due to scattering by dilute magnetic moments, and (iv) scattering of conduction electrons by structural two-level systems. In the present case, the first three explanations can be discarded based on the following arguments.

Quantum interference effects due to weak localization (i) are known to be very weak in magnetically ordered systems (although not zero) because of the destructive effect of the exchange field on the phase of the electron wave function on

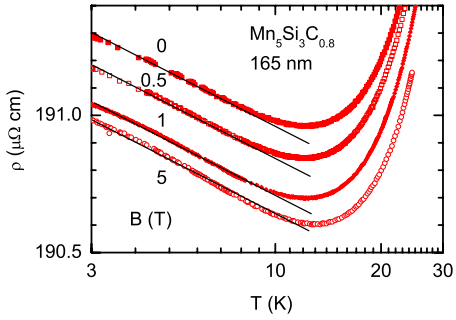

FIG. 8. (Color online) Semilogarithmic plot of $\rho(T)$ for a 165 nm $Mn_5Si_3C_{0.8}$ film (Table I, sample i) in various applied magnetic fields B applied perpendicularly to the film plane. Dashed-dotted lines indicate a linear dependence of constant slope.

time-reversed paths.[42] In three-dimensional disordered systems, the resistivity follows a $-T^{1/2}$ law.[43] A logarithmic dependence only appears in the two-dimensional regime, where the film is thinner than the phase-coherence length L_ϕ. This requirement is obviously hard to fulfill in films of 100–165 nm thickness. The same argument holds with regard to enhanced electron-electron interaction. In the two-dimensional regime, corrections due the conductivity $\Delta\sigma=-(\Delta\rho/\rho^2)d$ arising from weak localization and/or electron-electron interaction are of the order of the conductance quantum $L_{00}=e^2/\pi h=1.233\times10^{-5}\ \Omega^{-1}$ over one decade of T, i.e., the slope $\gamma=\frac{d\Delta\sigma}{d\ln T/T_{\min}}$ should be of the order of L_{00}.[43,44] In the present case, γ is roughly 1 order of magnitude larger than expected for weak localization and/or electron-electron interaction and increases with increasing thickness (see the films with $x=0.8$ in Table I). Furthermore, at low temperatures where the inelastic electron scattering rate τ_{in}^{-1} is usually smaller than $k_BT/\hbar$, both types of quantum corrections, weak localization and electron-electron interaction, are expected to change in weak magnetic fields.[43]

The single-ion magnetic Kondo effect can hardly occur in a material exhibiting long-range magnetic order. Any interaction between magnetic impurities leads to a strong reduction of the Kondo scattering eventually leading to spin-glass order. The most important experimental finding is the independence of the logarithmic slope on an applied magnetic field as large as 5 T. This points to a nonmagnetic origin of the scattering mechanism.

A logarithmic behavior of $\rho(T)$ was reported earlier by Cochrane *et al.*[45] for amorphous alloys. In disordered materials, a number of thermodynamic properties are successfully described by the tunneling model, where an atom (or a group of atoms) can tunnel between two different states of a double-well potential of height V and an energy splitting ΔE_{TLS} in configuration space, leading to low-energy excitations that can be modeled as two-level systems[46] and were also observed in amorphous metals.[47] Formally, the two-level system (TLS) can be considered as an impurity with pseudospin 1/2 coupled to the sea of conduction electrons. This orbital Kondo effect gives rise to a logarithmic increase of the resistivity around the Kondo temperature T_K as proposed by Zawadowski[48] and Vladár and Zawadowski.[49] Here, the spin degeneracy of the conduction electron provides two

channels.[50,51] The low-temperature resistivity behavior depends on the ratio $\Delta E_{\mathrm{TLS}}/k_B T_K$ (Ref. 50). For strict channel degeneracy—which is hard to realize experimentally—this leads to the two-channel Kondo effect[52] in the strong-coupling limit, i.e., for a frequently tunneling system and a strong scattering potential of the tunneling "impurity" $[\Delta E_{\mathrm{TLS}}(T) \ll k_B T_K]$. The coupling is enhanced if the tunneling atoms act as resonant scatterers at the Fermi level.[53] In the limit $\Delta E_{\mathrm{TLS}} \to 0$, the low-temperature physics is dominated by non-Fermi-liquid behavior $\rho \sim -T^{1/2}$ due to "overscreening" of the pseudospin. For finite splitting, a Fermi-liquid behavior $\rho \sim -T^2$ is recovered below T_K due to the complete screening of the TLS by the conduction electrons and the freezing-out of the electron-TLS scattering. The crossover occurs at $T_x \approx \Delta E_{\mathrm{TLS}}^2/k_B^2 T_K$. Eventually, the non-Fermi-liquid behavior vanishes for larger ΔE_{TLS}. In both cases, $\rho(T)$ shows a logarithmic behavior at higher T.

Experimental evidence for the presence of a two-channel Kondo effect has been reported for diamagnetic ThAsSe single crystals with an additional $-T^{1/2}$ term in the resistivity independent of magnetic field.[54] However, a saturation of $\rho(T)$ at very low temperatures was found to disappear in a weak magnetic field and was therefore attributed to quantum corrections arising from spin-orbit scattering. For other ThAsSe single crystals and $\mathrm{Ni}_x\mathrm{Nb}_{1-x}$ metallic glasses, a behavior $\sim -\ln T$ of the resistivity has been reported, again independent of magnetic field.[55,56] In both systems, the observed behavior points to electron scattering by TLS. Consequently, it is tempting to attribute the independence of the $-\ln T$ behavior from the magnetic field in $\mathrm{Mn_5Si_3C}_x$ films to an orbital Kondo effect derived from TLS.

In order to support this explanation, we have conducted resistivity measurements at temperatures below 1 K. Figure 9 shows $\rho(T,B) - \rho_{\mathrm{min}}(B)$, where $\rho_{\mathrm{min}}(B) = \rho(T_{\mathrm{min}}, B)$, in a semilogarithmic plot for the antiferromagnetic $\mathrm{Mn_5Si_3}$ film and for the ferromagnetic $\mathrm{Mn_5Si_3C_{0.8}}$ film in zero field and in $B = 5$ T applied perpendicularly to the surface. Remarkably, in both cases, the data aquired in zero field and in 5 T collapse onto the same curve, clearly demonstrating that the functional dependence of ρ with T does not change with magnetic field. Moreover, $\rho(T)$ saturates toward low temperatures reminiscent of Fermi-liquid behavior. Indeed, in both samples, a behavior $\Delta\rho \sim -T^2$ is observed below a crossover temperature $T_x \approx 0.5$ K, see insets of Fig. 9, independent of magnetic field. Interestingly, the behavior is independent of the type of magnetic order, antiferromagnetic, or ferromagnetic.

This suggests that the origin of the orbital Kondo effect is due to dynamical scatterers, for instance, precipitated C atoms located in the grain boundaries. From the high ρ_{min} and the failure of the Fuchs-Sondheimer model,[41] it is clear that the number of structural imperfections (grain boundaries, dislocations, and point defects) must be large. The temperature where half of the excess resistivity is reached (Fig. 9) yields an estimate of the Kondo temperature, $T_K \approx 1$ K for $\mathrm{Mn_5Si_3}$ and $T_K \approx 7$ K for $\mathrm{Mn_5Si_3C_{0.8}}$. The behavior is comparable to $\rho(T)$ of $\mathrm{Fe_{80}B_{20}}$-type amorphous alloys where the similar values of α (c.f., Table I) and T_K were observed.[45,57] From $\Delta E_{\mathrm{TLS}}^2 \approx k_B^2 T_x T_K$, a reasonable splitting ΔE_{TLS}

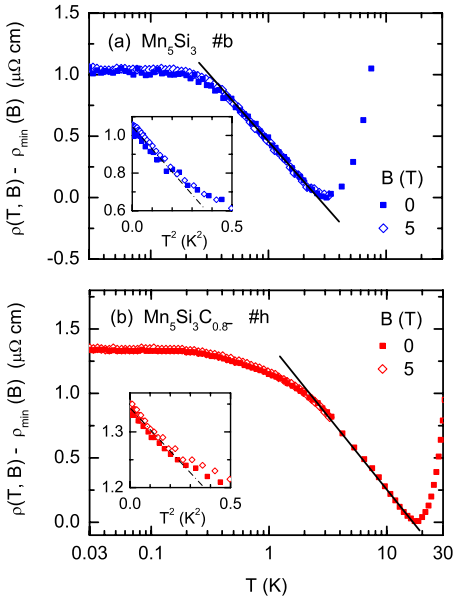

FIG. 9. (Color online) Semilogarithmic plot of the low-temperature resistivity $\rho(T,B)$ in zero field (closed symbols) and in 5 T (open symbols) with respect to the low temperature resistivity $\rho_{\mathrm{min}}(B) = \rho(T_{\mathrm{min}}, B)$ for (a) $\mathrm{Mn_5Si_3}$ and (b) $\mathrm{Mn_5Si_3C_{0.8}}$ films. Solid lines indicate a behavior $\sim -\ln T$. Insets show $\rho(T,B) - \rho_{\mathrm{min}}(B)$ vs T^2 where the dashed-dotted lines indicate a behavior $\sim -T^2$.

≈ 100 μeV is estimated. Consistently, a non-Fermi-liquid behavior is not observed. Note that the theory by Vladár and Zawadowski was developed for pure s-wave scattering, which differs from the case of itinerant s,p conduction electrons and more localized d electrons.

We conclude this section by reconsidering Fig. 5. The carbon concentration dependence of the parameters ρ_{min}, RRR, and α suggests that among the investigated $\mathrm{Mn_5Si_3C}_x$ films the cleanest behavior is observed for the antiferromagnetic $\mathrm{Mn_5Si_3}$ film and for ferromagnetic $\mathrm{Mn_5Si_3C}_x$ films with x close to 0.8. For these concentrations, the RRR is maximum associated with a minimum value of α representing the least amount of structural disorder. Hence, our results support the value of $x = 0.8$ as an optimum doping level as previously derived from magnetization data.

C. Magnetoresistance

Usually, the magnetoresistance (MR) of nonmagnetic metals and alloys is positive and follows Kohler's rule.[41] This ordinary magnetoresistance is due to orbital effects and increases $\sim B^2$. In magnetically ordered alloys, distinct differences of the MR are expected when comparing antiferromagnetically and ferromagnetically ordered materials.

The following data were taken by starting from a previously magnetized sample, i.e., from the remanent state, after application of a magnetic field much larger than the typical saturation fields observed in $M(T)$, c.f., Fig. 3(b), but smaller than $B = 11$ T for which a metamagnetic transition occurs in bulk $\mathrm{Mn_5Si_3}$.[24] Figure 10 shows the relative magnetoresistance $\mathrm{MR} = [\rho(B) - \rho(0)]/\rho(0)$ at $T = 4.2$ K for (a) antiferromagnetic $\mathrm{Mn_5Si_3}$ and (b) ferromagnetic $\mathrm{Mn_5Si_3C_{0.8}}$ films in a

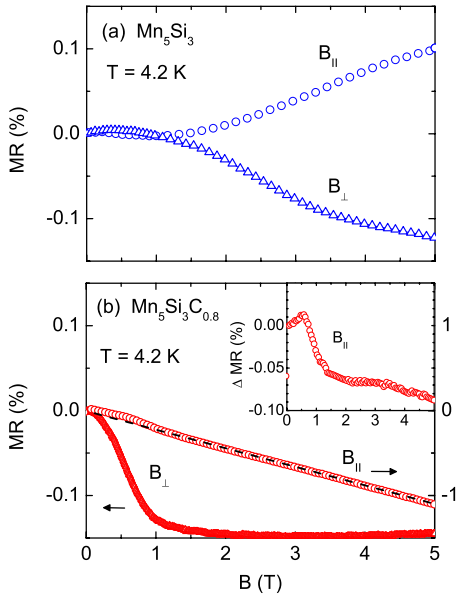

FIG. 10. (Color online) Relative magnetoresistance MR=$[\rho(B)-\rho(0)]/\rho(0)$ vs applied magnetic field B for (a) antiferromagnetic Mn_5Si_3 and (b) ferromagnetic $Mn_5Si_3C_{0.8}$ films. Inset shows the MR($B_\parallel$ for $Mn_5Si_3C_{0.8}$ after subtraction of the linear "background" indicated by the dashed line in (b).

magnetic field B applied in plane along the sample strip ($B_\parallel$) or perpendicularly to the plane ($B_\perp$) and with the current parallel to the length of the strip.

For the antiferromagnetic undoped Mn_5Si_3 film, the transverse MR($B_\perp$) is negative apart from a very weak positive contribution for fields below 1 T. The longitudinal MR($B_\parallel$) is positive for fields larger than 1.5 T. This behavior is in qualitative agreement with the calculated MR of an antiferromagnet with *s-d* interaction for which a behavior MR$\sim -B_\perp$ and MR$\sim B_\parallel^2$ is expected.[58]

In contrast, the MR of the ferromagnetic $Mn_5Si_3C_{0.8}$ film is negative for both field orientations [Fig. 10(b)]. Note that in this case, the in-plane contribution is a factor of 10 larger than the out-of-plane contribution. The result MR($B_\parallel$) $\gg$MR($B_\perp$) is often experimentally observed for strong *s-d* scattering due to anisotropic spin-orbit interaction.[41] MR($B_\parallel$) reveals an additional contribution at low fields besides the roughly linear behavior indicated by the dashed line. If the linear behavior is subtracted from the total MR, the behavior of the residual part [inset Fig. 10(b)] resembles MR($B_\perp$) with similar magnitude and saturation field.

A small negative transverse MR in ferromagnets is usually explained by domain-wall motion, where the alignment of ferromagnetic domains in the field leads to a lower spin-dependent scattering of electrons between the different domains, similar to the giantmagnetoresistance (GMR) effect. A GMR-like MR has been reported even for chemically homogeneous films with perpendicular magnetic anisotropy such as hcp (0001)-oriented Co films or FePd alloy films.[59,60] A GMR-like contribution is also present in the longitudinal MR($B_\parallel$) [inset Fig. 10(b)] which is, however, dominated by a much larger roughly linear decrease with increasing field. A negative and linear longitudinal MR without saturation was also reported for Fe, Co, and Ni films.[61] In that case, the MR was calculated following the early work of Goodings[40] by taking into account intraband (*s-s*,*d-d*) and interband (*s-d*) spin-flip electronic transitions due to electron–spin-wave scattering.[61] The high-field MR was assigned to the damping of spin waves by the external field which reduces the electron–spin-wave scattering.

In conclusion, although the observed MR of $Mn_5Si_3C_x$ films with $x=0$ and 0.8 are small, it shows distinct qualitative differences due to the different kinds of magnetic order in these films. The perpendicular MR seems to be dominated by spin-dependent scattering in the magnetically ordered material rather than by the orbital Kondo effect discussed in Sec. III B 2.

D. Hall effect

The ordinary Hall effect in a perpendicular magnetic field is given by $\rho_{HE}=R_0B$ with the Hall coefficient $R_0=1/ne$ assuming one type of charge carriers of density n. However, in the presence of different types of carriers like in semiconductors, semimetals, or transition metals, R_0 is better approximated by a two-band model.

In magnetically ordered materials, an additional contribution due to the extraordinary or anomalous Hall effect (AHE)

$$\rho_{\text{Hall}} = \rho_{\text{HE}} + \rho_{\text{AHE}} = R_0B + R_S\mu_0M \tag{6}$$

exists, where R_S is the anomalous Hall coefficient. R_S is due to an asymmetric diffusion of charge carriers arising from spin-orbit coupling and is often separated into two contributions attributed to (i) skew scattering and (ii) side jumps. The AHE is related to the longitudinal resistivity by $R_S=a(M)\rho+b(M)\rho^2$,[62] where the linear term is attributed to skew scattering alone and the second term arises from the side-jump mechanism with a possible contribution from skew scattering as well. In ferromagnets, the low-field Hall effect is dominated by the field dependent magnetization $M(B)$, whereas the ordinary Hall coefficient can be determined by extrapolating the high-field data, where the magnetization is saturated, to $\rho_{\text{Hall}}(B=0)$.

Figure 11 shows the Hall resistivity for antiferromagnetic Mn_5Si_3 and ferromagnetic $Mn_5Si_3C_{0.8}$ films measured with a probing current of $I=10$ μA at $T=4.2$ K. In antiferrromagnetic Mn_5Si_3, an ordinary Hall effect with a positive slope $R_0=0.025$ $\mu\Omega$ cm/T is observed. This demonstrates that the AHE is negligible as expected from the very small $M(B)$ in the antiferromagnetic case. For a single band, R_0 corresponds to a density of holes $n_h=2.5\times10^{22}$ cm^{-3}, i.e., to roughly 0.5 holes per Mn_5Si_3 unit cell. However, in the present case, different electronic bands arising from Si and Mn states contribute to electronic transport. Therefore, a two-band model of *s*- and *d*-conduction electrons with different carrier densities and mobilities would be more appropriate. Unfortunately, these parameters are presently unknown which prevents a further analysis. We mention that a positive Hall effect was also observed for antiferromagnetic α-Mn.[63]

In contrast to the normal Hall effect of the antiferromagnetic Mn_5Si_3 film, an anomalous Hall effect is observed for the $Mn_5Si_3C_{0.8}$ film as expected for a ferromagnetically or-

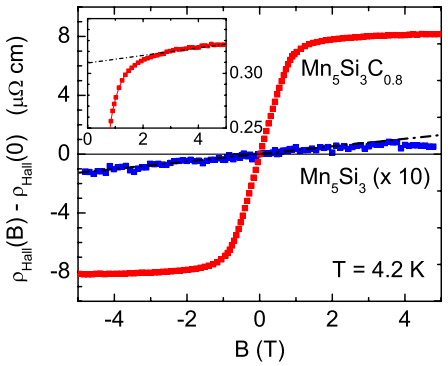

FIG. 11. (Color online) Hall resistivity $\rho_{\mathrm{Hall}}(B)-\rho_{\mathrm{Hall}}(0)$ vs applied magnetic field B for antiferromagnetic Mn_5Si_3 (ten times) and ferromagnetic $Mn_5Si_3C_{0.8}$ films ($d=100$ nm). Inset shows the Hall resistivity for $Mn_5Si_3C_{0.8}$ at high fields. Dash-dotted lines indicate a linear behavior.

dered material with a field dependent magnetization $M(B)$. For the Hall effect, the field is always oriented along the surface normal, i.e., along the magnetically hard axis. Therefore, no coercivity is observed in this case. The strong anomalous contribution $\sim R_S$ saturates for fields above ≈ 1 T similar to the saturation of the transverse resistivity $\rho(B_\perp)$ [see Fig. 10(b)]. From the slope of $\rho_{\mathrm{Hall}}(B)$ after M has saturated, we obtain a positive $R_0 \approx 0.03 \pm 0.01$ $\mu\Omega$ cm/T (inset Fig. 11), nearly the same value as for the undoped material. This indicates that the carrier density does not change considerably with carbon concentration x. The behavior is fundamentally different from the Hall effect of epitaxial Mn_5Ge_3 films[26] where at low T a negative and much larger $R_0=-0.38$ $\mu\Omega$ cm/T can be extracted [see Fig. 2(a) of Ref. 26]. Clearly, a detailed investigation of the Hall effect requires further measurements at different temperatures.

IV. SUMMARY

In $Mn_5Si_3C_x$ films, the magnetic order changes from antiferromagnetic ($x=0$) to ferromagnetic ($x \geqslant 0.2$). The concentration dependence of the magnetic properties seems to be dominated by the changes of interatomic distances and corresponding bondings, in particular, with regard to the sensitive dependence of Mn moments on their local atomic environment. High resistivities appear to be characteristic of these Mn-metaloid compounds and are possibly due to the partially localized d electrons with a high electronic density of states and strong s-d scattering. For temperatures $T > 10-20$ K (depending on film thickness d), the resistivity $\rho(T)$, magnetoresistance, and Hall effect can be qualitatively described by available theories that take into account s-d as well as electron–spin-wave scattering. At low temperatures, $\rho(T)$ is dominated by a logarithmic T-dependence characteristic for scattering of conduction electrons by two-level systems with a crossover to a Fermi-liquid behavior below ≈ 1 K. Remarkably, this low-temperature behavior is independent of the type of magnetic order, viz., ferromagnetic or antiferromagnetic.

ACKNOWLEDGMENTS

This work was supported through the Graduiertenkolleg "Komplexe Phänomene im Festkörper" (B.G.) and the Alexander von Humboldt Stiftung (A.S.). We thank G. Fischer for performing some magnetization measurements.

*Present address: 3. Physikalisches Institut, Universität Stuttgart, D-70569 Stuttgart, Germany.
†On leave from the Bhabha Atomic Research Center (BARC), Mumbai 400 085, India.

[1] T. Dietl, H. Ohno, F. Matsukara, J. Cibert, and D. Ferrand, Science **287**, 1019 (2002).
[2] F. M. Zhang, X. C. Liu, J. Gao, X. S. Wu, Y. W. Du, H. Zhu, J. Q. Xiao, and P. Chen, Appl. Phys. Lett. **85**, 786 (2004).
[3] Y. D. Park, A. T. Hanbicki, S. C. Erwin, C. S. Hellberg, J. M. Sullivan, J. E. Mattson, T. F. Ambrose, A. Wilson, G. Spanos, and B. T. Jonker, Science **295**, 651 (2002).
[4] S. Zhou, K. Potzger, G. Zhang, A. Mücklich, F. Eichhorn, N. Schell, R. Grötzschel, B. Schmidt, W. Skorupa, M. Helm, J. Fassbender, and D. Geiger, Phys. Rev. B **75**, 085203 (2007).
[5] C. Bihler, C. Jaeger, T. Vallaitis, M. Gjukic, M. S. Brandt, E. Pippel, J. Woltersdorf, and U. Gösele, Appl. Phys. Lett. **88**, 112506 (2006).
[6] C. Zeng, S. C. Erwin, L. C. Feldman, A. P. Li, R. Jin, Y. Song, J. R. Thompson, and H. H. Weitering, Appl. Phys. Lett. **83**, 5002 (2003).
[7] S. Picozzi, A. Continenza, and A. J. Freeman, Phys. Rev. B **70**, 235205 (2004).
[8] Y. Zhang, A. P. Runge, Z. S. Shan, and D. J. Sellmyer, J. Appl. Phys. **75**, 6354 (1994).
[9] E. Sawatzky, J. Appl. Phys. **42**, 1706 (1971).
[10] G. H. Lander, P. J. Brown, and J. B. Forsyth, Proc. Phys. Soc. London **91**, 332 (1967).
[11] P. Brown and J. Forsyth, J. Phys.: Condens. Matter **7**, 7619 (1995).
[12] M. Ramos Silva, P. J. Brown, and J. B. Forsyth, J. Phys.: Condens. Matter **14**, 8707 (2002) and references therein.
[13] B. Forsyth and P. J. Brown, J. Phys.: Condens. Matter **2**, 2713 (1990).
[14] A. Stroppa and M. Peressi, Phys. Status Solidi A **204**, 44 (2007).
[15] J. P. Sénateur, J.-P. Bouchaud, and R. Fruchart, Bull. Soc. Fr. Mineral. Cristallogr. **90**, 537 (1967).
[16] T. Takeuchi, M. Igarashi, Y. Hirayama, and M. Futamoto, J. Appl. Phys. **78**, 2132 (1995).
[17] R. Nakatani, T. Kusano, H. Yakame, and M. Yamamoto, Jpn. J. Appl. Phys., Part 1 **41**, 5978 (2002).
[18] W. Wang, F. Takano, H. Akinaga, and H. Ofuchi, Phys. Rev. B **75**, 165323 (2007).
[19] C. Sürgers, M. Gajdzik, G. Fischer, H. v. Löhneysen, E. Welter, and K. Attenkofer, Phys. Rev. B **68**, 174423 (2003).
[20] M. Gajdzik, C. Sürgers, M. Kelemen, and H. v. Löhneysen, J. Magn. Magn. Mater. **221**, 248 (2000).

[21] M. Gajdzik, C. Sürgers, M. Kelemen, and H. v. Löhneysen, J. Appl. Phys. **87**, 6013 (2000).
[22] H. von Löhneysen, A. Neubert, T. Pietrus, A. Schröder, O. Stockert, U. Tutsch, M. Loewenhaupt, A. Rosch, and P. Wölfle, Eur. Phys. J. B **5**, 447 (1998).
[23] R. Haug, G. Kappel, and A. Jaéglé, Phys. Status Solidi A **55**, 285 (1979).
[24] L. Vinokurova, V. Ivanov, E. Kulatov, and A. Vlasov, J. Magn. Magn. Mater. **90&91**, 121 (1990).
[25] I. A. Campbell and A. Fert, in *Ferromagnetic Materials*, edited by E. P. Wohlfarth (North-Holland, Amsterdam, 1982), Vol. 3, p. 747.
[26] C. Zeng, Y. Yao, Q. Niu, and H. H. Weitering, Phys. Rev. Lett. **96**, 037204 (2006).
[27] N. F. Mott, Adv. Phys. **13**, 325 (1964).
[28] A. Irizawa, A. Yamasaki, M. Okazaki, S. Kasai, A. Sekiyama, S. Imada, S. Suga, E. Kulatov, H. Ohta, and T. Nanba, Solid State Commun. **124**, 1 (2002).
[29] G. Grimvall, *Thermophysical Properties of Materials* (Elsevier Science, Amsterdam, 1999), p. 245.
[30] G. I. Kalishevich, N. P. Sudakova, A. V. Mikhel'son, N. V. Gel'd, and V. I. Surikov, Sov. Phys. Solid State **16**, 1386 (1975).
[31] For a review see O. Gunnarsson, M. Calandra, and J. E. Han, Rev. Mod. Phys. **75**, 1085 (2003).
[32] G. T. Meaden, Contemp. Phys. **12**, 313 (1971).
[33] M. A. Continentino, Phys. Rev. B **73**, 132406 (2006).
[34] H. Yamada and S. Takada, J. Phys. Soc. Jpn. **34**, 51 (1973).
[35] K. Ueda, J. Phys. Soc. Jpn. **43**, 1497 (1977).
[36] T. Kasuya, Prog. Theor. Phys. **22**, 227 (1959).
[37] I. Mannari, Prog. Theor. Phys. **22**, 335 (1959).
[38] C. Pfleiderer, G. J. McMullan, S. R. Julian, and G. G. Lonzarich, Phys. Rev. B **55**, 8330 (1997).
[39] A. R. Makintosh, Phys. Lett. **4**, 140 (1963).
[40] D. A. Goodings, Phys. Rev. **132**, 542 (1963).
[41] T. R. McGuire and R. I. Potter, IEEE Trans. Magn. **11**, 1018 (1975).
[42] For an overview see F. G. Aliev, V. K. Dugaev, and J. Barnaś, in *Encyclopedia of Nanoscience and Nanotechnology*, edited by H. S. Nalwa (American Scientific, Valencia, 2004), Vol. 4, p. 587.
[43] P. A. Lee and T. V. Ramakrishnan, Rev. Mod. Phys. **57**, 287 (1985).
[44] G. Bergmann, Phys. Rep. **107**, 2 (1984).
[45] R. W. Cochrane, R. Harris, J. O. Ström-Olson, and M. J. Zuckermann, Phys. Rev. Lett. **35**, 676 (1975).
[46] *Amorphous Solids*, edited by W. A. Phillips (Springer, Berlin, 1981).
[47] H. v. Löhneysen, Phys. Rep. **79**, 161 (1981).
[48] A. Zawadowski, Phys. Rev. Lett. **45**, 211 (1980).
[49] K. Vladár and A. Zawadowski, Phys. Rev. B **28**, 1564 (1983); **28**, 1582 (1983); **28**, 1596 (1983).
[50] D. L. Cox and A. Zawadowski, Adv. Phys. **47**, 599 (1998).
[51] J. von Delft, D. C. Ralph, R. A. Buhrman, S. K. Upadhyay, R. N. Louie, A. W. W. Ludwig, and V. Ambegaokar, Ann. Phys. (N.Y.) **263**, 1 (1998).
[52] P. Nozières and A. Blandin, J. Phys. (Paris) **41**, 193 (1980).
[53] G. Zaránd, Phys. Rev. B **72**, 245103 (2005).
[54] T. Cichorek, A. Sanchez, P. Gegenwart, F. Weickert, A. Wojakowski, Z. Henkie, G. Auffermann, S. Paschen, R. Kniep, and F. Steglich, Phys. Rev. Lett. **94**, 236603 (2005).
[55] T. Cichorek, H. Aoki, J. Custers, P. Gegenwart, F. Steglich, Z. Henkie, E. D. Bauer, and M. B. Maple, Phys. Rev. B **68**, 144411 (2003).
[56] A. Halbritter, O. Yu. Kolesnychenko, G. Mihály, O. I. Shklyarevskii, and H. van Kempen, Phys. Rev. B **61**, 5846 (2000).
[57] Ö. Rapp J. E. Grinberg, and K. V. Rao, J. Appl. Phys. **49**, 1733 (1978).
[58] H. Yamada and S. Takada, Prog. Theor. Phys. **49**, 1401 (1973).
[59] J. F. Gregg, W. Allen, K. Ounadjela, M. Viret, M. Hehn, S. M. Thompson, and J. M. D. Coey, Phys. Rev. Lett. **77**, 1580 (1996).
[60] D. Ravelosona, A. Cebollada, F. Briones, C. Diaz-Paniagua, M. A. Hidalgo, and F. Batallan, Phys. Rev. B **59**, 4322 (1999).
[61] B. Raquet, M. Viret, E. Sondergard, O. Cespedes, and R. Mamy, Phys. Rev. B **66**, 024433 (2002).
[62] A. Gerber, A. Milner, A. Finkler, M. Karpovski, L. Goldsmith, J. Tuaillon-Combes, O. Boisron, P. Mélinon, and A. Perez, Phys. Rev. B **69**, 224403 (2004).
[63] A. D. C. Grassie and K. G. Adanu, Solid State Commun. **24**, 345 (1977).